Atmospheric and Oceanic Science Letters 18 (2025) 100666

Contents lists available at ScienceDirect

Atmospheric and Oceanic Science Letters

journal homepage:
http://www.keaipublishing.com/en/journals/atmospheric-and-oceanic-science-letters/

Synoptic background conditions and moisture transport for producing the extreme heavy rainfall event in Valencia in 2024

Tingting Huang[a,b], Shenming Fu[a,c,*], Xiao Li[d], You Dong[e], Yuanchun Zhang[f], Jianhua Sun[a]

[a] Laboratory of Cloud–Precipitation Physics and Severe Storms, Institute of Atmospheric Physics, Chinese Academy of Sciences, Beijing, China
[b] University of Chinese Academy of Sciences, Beijing, China
[c] State Key Laboratory of Earth System Numerical Modeling and Application, Institute of Atmospheric Physics, Chinese Academy of Sciences, Beijing, China
[d] School of Civil Engineering, Chongqing University, Chongqing, China
[e] Department of Civil and Environmental Engineering, The Hong Kong Polytechnic University, Hong Kong, China
[f] State Key Laboratory of Atmospheric Environment and Extreme Meteorology, Institute of Atmospheric Physics, Chinese Academy of Sciences, Beijing, China

ARTICLE INFO

Keywords:
Spain
Mediterranean
Valencia
Moisture budget
Extreme heavy rainfall
Lagrangian circulation/transport

关键词:
西班牙
地中海
瓦伦西亚
水汽收支
极端强降雨
拉格朗日环流/输送

ABSTRACT

From 26 October to 2 November 2024, Spain experienced a record-breaking rainfall event, with the most intense episode appearing in Valencia Province. During the event, Turis station recorded a historic 24-hour precipitation of 710.8 mm, exceeding the national annual average. This resulting flood led to widespread disruption and significant societal impacts. Synoptic analyses reveal that the event was dominated by a deep cut-off low extending through the entire troposphere and persisting for approximately 186 h. Background conditions were characterized by upper-level divergence, mid-tropospheric warm advection, and a strong southeasterly low-level jet, which promoted vertical motion and sustained moisture transport. The steep, funnel-shaped terrain along the eastern Iberian coast further triggered and enhanced the local convection. A 10-day backward Lagrangian moisture tracing using the HYSPLIT model identified the Mediterranean Sea as the primary moisture source (78.1 %), followed by northwestern Africa (8.5 %) and central-eastern Europe/the Black Sea (6.2 %). Low-level moisture transport was mainly driven by the cut-off low and a persistent Mediterranean high, while mid- to upper-level trajectories were associated with a preceding low-pressure system over the Mediterranean and the subtropical Atlantic high. These systems acted in sequence to relay moisture toward the Valencia region, and under the influence of the strongly rotating and convergent cut-off low—along with terrain-induced lifting—this moisture was rapidly uplifted, ultimately triggering the extreme rainfall event.

摘要

2024年10月26日至11月2日, 西班牙瓦伦西亚省遭遇罕见极端降雨, Turis站24小时降水量达710.8毫米, 引发严重洪涝灾害. 此次事件由持续186小时的深厚切断低压主导, 在高层辐散, 中层暖平流与低空东南急流共同作用下形成强垂直运动, 东海岸漏斗地形进一步增强对流. HYSPLIT后向追踪显示, 水汽主要来自地中海 (贡献率78.1 %), 其次为非洲西北部 (8.5 %) 和欧洲中东部/黑海 (6.2 %). 水汽由多个天气系统接力输送至瓦伦西亚, 最终在切断低压旋转辐合和地形抬升作用下, 引发此次破纪录降雨事件.

1. Introduction

Extreme rainfall and floods are recurrent hazards in Mediterranean countries, particularly in densely populated coastal zones, which are especially vulnerable during late summer and autumn (Riesco Martin et al., 2013). The province of Valencia, on the eastern flank of the Iberian Peninsula, is particularly prone to such events (Insua-Costa et al., 2021). Geographically, the region is bordered to the west by the Iberian Mountains, which rise above 2000 m, while to the east it opens into the Mediterranean Sea via a broad lowland plain. This "funnel-shaped" terrain (Fig. 1(a)) channels moist easterly winds inland, enhancing topographic lifting and convergence, thus creating conditions favorable for intense convective rainfall. Historical events underscore the region's vulnerability to high-impact rainfall. For instance, the catastrophic "Great Valencia Flood" in October 1957 brought 446 mm of rainfall in 48 h at Lliria station, resulting in levee breaches and 81 deaths (Portugues-Molla et al., 2016; Puertes and Francés García, 2016). Similarly, in October 1982, 426 mm of rainfall at Cofrentes triggered dam failures and

* Corresponding author.
E-mail address: fusm@mail.iap.ac.cn (S. Fu).

https://doi.org/10.1016/j.aosl.2025.100666
Received 20 April 2025; Revised 5 June 2025; Accepted 16 June 2025
Available online 18 June 2025
1674-2834/© 2025 The Authors. Publishing Services by Elsevier B.V. on behalf of KeAi Communications Co. Ltd. This is an open access article under the CC BY-NC-ND license (http://creativecommons.org/licenses/by-nc-nd/4.0/)

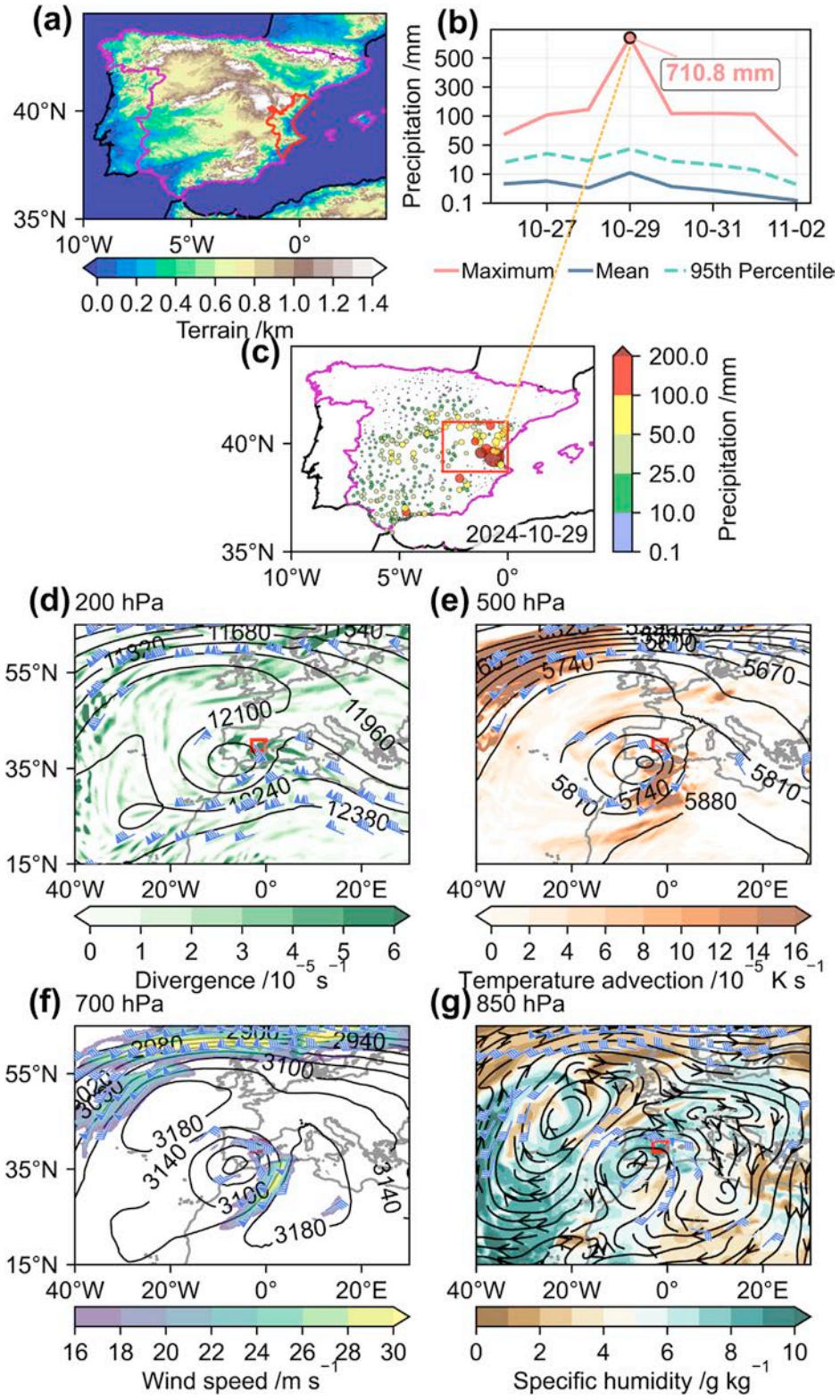

Fig. 1. The topography, precipitation distribution, and synoptic conditions associated with the extreme rainfall event in Spain from 26 October to 2 November 2024. (a) Topography of Spain and surrounding regions, with the red outline marking Valencia Province. (b) Maximum, average, and 95th percentile of 24-hour accumulated precipitation (from 0700 UTC of the previous day to 0600 UTC) during the event period. The dot and label indicate the timing and amount of the maximum 24-hour precipitation, and the orange dashed line points to the corresponding station in (c). (c) Distribution of 24-hour accumulated precipitation on 29 October 2024, where color and marker size indicate amounts; the red rectangle highlights the area of most intense rainfall. In (a) and (c), black solid lines indicate coastlines, dashed black lines show national borders, and the purple line marks Spain's boundary. (d–g) Synoptic fields at 1800 UTC 29 October 2024, including geopotential height (black solid lines), divergence (shaded), temperature advection (shaded), wind speed (shaded), specific humidity (shaded), and flow field at 200, 500, 700, and 850 hPa levels. Wind barbs denote wind speeds exceeding level-specific thresholds: 25 m s^{-1} at 200 hPa, 16 m s^{-1} at 500 and 700 hPa, and 12 m s^{-1} at 850 hPa.

widespread flooding along the Júcar River, resulting in over 40 fatalities and $630 million in damages (Barredo, 2007). More recently, in September 2019, Orihuela reported 492 mm of rainfall, reported 7 deaths and damages exceeding €425 million (Amengual, 2022; Hermoso et al., 2021).

Moisture is a key prerequisite for extreme precipitation (Tao, 1980), and both its supply and transport play a central role in driving high-impact rainfall events (Khodayar et al., 2018). Therefore, understanding the origin and transport pathways of moisture has become a critical focus in extreme rainfall research (Huang et al., 2024, 2025). Approximately 90 % of atmospheric moisture originates from oceanic and continental water bodies (Quante and Matthias, 2006), and reaches precipitation zones through atmospheric advection. Three main sources typically contribute to rainfall: remote transport, pre-existing humidity, and local surface evaporation, with their relative importance varying significantly across events. Insua-Costa et al. (2019) used WRF model simulations to investigate two major flood events over the western Mediterranean in autumn 1982. They found that in October, both long-range transport and local evaporation contributed comparably to rainfall, whereas in November, remote sources dominated. Moisture sources can vary significantly even within a single region. The Iberian Peninsula, located between two major vapor reservoirs—the Atlantic Ocean and the Mediterranean Sea—experiences seasonal fluctuations in their relative influence. During spring and summer, local and regional evaporation predominates, while in autumn and winter, moisture is often advected from the subtropical Atlantic through the North Atlantic moisture corridor (Gimeno et al., 2010). Additionally, studies have shown that the Bay of Biscay contributes significantly to rainfall over the Galician/northern Portugal region under anticyclonic conditions (Drumond et al., 2011). Wind direction has also been identified as a key factor: southeasterly winds typically enhance coastal rainfall, while southerly flows tend to shift precipitation inland (Javier Miro et al., 2022).

Recent studies suggest a general decline in mean precipitation along Spain's Mediterranean coast, coupled with increasing trends and high uncertainty in both droughts and extreme rainfall events (Beneto and Khodayar, 2023). An unprecedented extreme rainfall event struck Spain between 26 October and 2 November 2024. On 29 October, Turis station in Valencia recorded 710.8 mm of rain—more than the country's average annual rainfall—leading to 232 fatalities, affecting over 36 000 people, and causing economic losses estimated at $11 billion (https://public.emdat.be/data [Accessed 2025–04–12]). Given the magnitude and societal impact of this event, a focused case study is essential to understand the mechanisms and moisture dynamics involved. Insights gained will help inform risk assessments for similar regions across the Mediterranean. This study focuses on the moisture sources and transport pathways associated with the 2024 Valencia event, addressing the following key questions: (a) What were the dominant moisture source regions? (b) What were the quantitative contributions and transport characteristics of each source? (c) Which synoptic-scale systems governed the anomalous moisture transport? To answer these questions, we combine synoptic diagnostics with a Lagrangian moisture tracing approach.

The remainder of this paper is structured as follows: Section 2 describes the data and methods; Section 3 provides an event overview; Section 4 examines moisture source regions and transport patterns from a Lagrangian perspective; Section 5 explores the governing synoptic systems; and Section 6 provides the conclusions and some further discussion.

2. Data and methods

2.1. Data

This study utilizes four datasets: (i) daily accumulated precipitation data from 947 gauges provided by the Spanish Meteorological Agency (AEMET), which are used to analyze temporal and spatial precipitation distributions; (ii) hourly reanalysis products at a resolution of 0.25° × 0.25° from the fifth major global reanalysis produced by ECMWF (ERA5; Hersbach et al., 2020), which are used to investigate the large-scale circulation patterns and synoptic systems, as well as to drive the HYSPLIT model for backward moisture tracking; (iii) topographic data at a resolution of 15″ × 15″ (arc-seconds) from the General Bathymetric Chart of the Oceans (GEBCO; https://www.gebco.net/data_and_products/gridded_bathymetry_data [Accessed 2024–11–12]).

2.2. Backward trajectory simulations and quantification of moisture source contributions

We used the HYSPLIT model to conduct 10-day backward trajectory simulations from the peak of the rainfall event on 29 October 2024, driven by ERA5 data from the surface to 300 hPa. Based on the observed rainfall maximum (Fig. 1(c)), we defined the target region (38.7°–41°N, 3°W–0°) and initialized 51 239 particles on a uniform 0.25° × 0.25° horizontal grid across the domain. Following Stohl et al. (2008), target particles were identified by a significant decrease in specific humidity within the first three hours of backward tracking, indicating moisture release within the target region. A total of 26 697 particles met this criterion and were used for further analysis.

Following Stohl and James (2004, 2005), the moisture budget is diagnosed from the temporal changes in specific humidity:

$$E - P \approx \frac{\sum_{i=1}^{N} \left(m_i \frac{\mathrm{d}q_i}{\mathrm{d}t} \right)}{A},$$

where E and P are the evaporation and precipitation rates per unit area, m_i is the mass of the parcel, and $\mathrm{d}q_i/\mathrm{d}t$ is the rate of change in specific humidity. In the HYSPLIT model, each parcel's mass is assumed to be 1 kg. We use a 1° × 1° grid as area A and calculate $\mathrm{d}q/\mathrm{d}t$ from the HYSPLIT output to estimate $E - P$. Based on Trenberth and Stepaniak (2003) and Stohl and James (2004), evaporation and precipitation rarely occur simultaneously. In this context, when $E - P \gg 0$, evaporation dominates and the region acts as a moisture source. Conversely, when $E - P \ll 0$, precipitation dominates and the region acts as a moisture sink. The E–P distribution helps identify potential moisture sources for the extreme rainfall event.

To quantify the relative contributions of different source regions and examine moisture transport pathways, we applied the areal source–receptor attribution method proposed by Sun and Wang (2014). Full methodological details are provided in the Supplementary Material.

3. Overview of the event

From 26 October to 2 November 2024, Spain experienced persistent heavy rainfall, with both the average and 95th percentile of 24-hour accumulated rainfall remaining exceptionally high, peaking on 27 and 29 October (Fig. 1(b)). Throughout this period, 24-hour rainfall consistently exceeded 50 mm, with 29 October standing out. On this day, Turis station in Valencia recorded a staggering 710.8 mm—more than its annual average—setting a new historical rainfall record. The storm's impact was widespread, affecting nearly the entire country, with Valencia at the storm's center (Fig. 1(c)). The event resulted in severe flooding, 232 fatalities, numerous injuries, and enormous economic losses.

On 29 October, at 200 and 500 hPa, a deep cut-off low centered over the Iberian Peninsula was flanked by ridges over the eastern Atlantic and North Africa (Fig. 1(d, e)). At 700 and 850 hPa, these ridges developed into a high-pressure system with clockwise circulation (Fig. 1(f, g), forming a blocked pattern that contributed to the persistence of the cut-off low. The primary driver of this extreme event was a cut-off low that detached from the midlatitude westerlies over northern Spain around 0500 UTC on 26 October, gradually deepened while remaining quasi-stationary, and finally dissipated over northwestern Africa around 2200

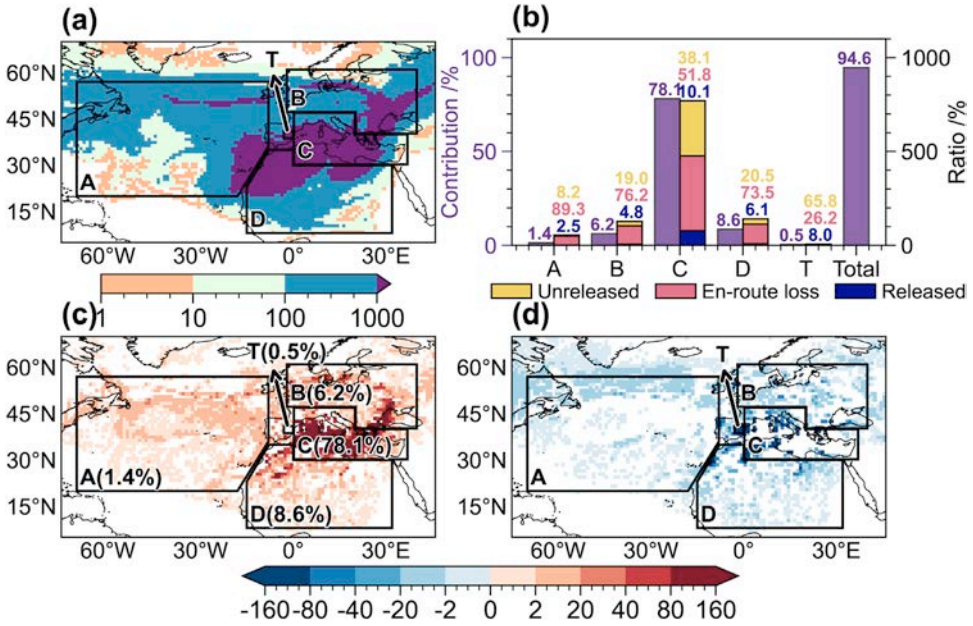

Fig. 2. Frequency distribution of backward trajectories and moisture source contributions. (a) Frequency distribution (shaded) of backward trajectories on a 1° × 1° grid. Black polygons outline moisture source regions (A–T), including the northern Atlantic (A), central-eastern Europe/the Black Sea (B), Mediterranean (C), northern Africa (D), and the target rainfall area in Spain (T). (b) Contribution of each moisture source region and total contribution (left purple bars), with moisture uptake components (unreleased, enroute loss, and released) as percentages of total uptake. (c) Evaporation zones ($E - P > 0$; shading, units: mm), with moisture contributions from each source. (d) Precipitation zone ($E - P < 0$; shading, units: mm).

UTC 2 November—lasting approximately 186 h (Fig. S1 in the Supplementary Material). The most intense rainfall occurred on 29 October, coinciding with the mature phase of the cut-off low. At that time, strong upper-level divergence, mid-level warm advection, and a southeasterly low-level jet prevailed over eastern Spain (Fig. 1). According to quasi-geostrophic theory and the continuity equation, upper-level divergence and mid-level warm advection enhanced vertical ascent (Holton and Hakim, 2013a, b), while the southeasterly low-level jet continuously transported the moisture from the Mediterranean toward the Valencia region, resulting in strong mass and moisture convergence (Ricard et al., 2012). Importantly, the steep funnel-shaped terrain along the eastern Iberian coast further amplified orographic lifting as it interacted with the low-level jet (Fig. S2 in the Supplementary Material), helping to focus rainfall over the Valencia area. This vertical configuration supported persistent deep convection and extreme precipitation through enhanced latent heat release (Fu et al., 2017).

4. Lagrangian moisture budget

Trajectories showing a specific humidity drop greater than 1 g kg^{-1} within the first three hours (26 697 in total) were defined as target trajectories, representing key contributors to precipitation. The target trajectories were densely concentrated over the eastern North Atlantic, Europe, the Mediterranean, and northwestern Africa (Fig. 2(a)), suggesting that these regions were likely potential moisture source areas.

To quantify surface moisture uptake and release, we calculated $E - P$ values along the trajectories on a 1° × 1° grid and display the net evaporation ($E - P > 0$) and net precipitation ($E - P < 0$) separately to distinguish source and precipitation regions (Fig. 2(c, d)). Strong moisture uptake is evident over the Mediterranean, Europe, the Atlantic, and northern Africa, while the target region, Valencia, exhibits intense moisture release, which is consistent with the observed distribution. Based on both trajectory density and $E - P$ patterns, we identified four major moisture uptake regions (A–D, outlined in Fig. 2(a, f, g): the northern Atlantic (A); central-eastern Europe/the Black Sea (B); the Mediterranean (C); and northern Africa (D)). The rainfall region (T) was also included as a potential local source.

The contribution of each region was quantified using the areal–source–receptor attribution method (Sun and Wang, 2014; Fig. 2(b)). Together, these regions accounted for 94.6 % of the total moisture, providing a strong explanation for the event's moisture sources. The Mediterranean dominates (C; 78.1 %) due to its high moisture uptake, relatively low enroute loss (48.2 %), and high release efficiency (10.1 %). Northern Africa (D; 8.5 %) and central-eastern Europe/the Black Sea (B; 6.2 %) contributed moderately, with region D being more effective due to lower transport loss and greater release. Contributions from the distant Atlantic (A; 1.4 %) and the local source (T; 0.5 %) were minimal, limited by substantial enroute loss and low release, respectively.

In summary, the Mediterranean served as the primary moisture source, supported by abundant oceanic supply, efficient transport, and strong release near the target region. Continental sources provided limited support, while remote and local inputs were minimal.

5. Controlling synoptic systems

To investigate the synoptic systems governing moisture transport during the 10-day backward trajectory analysis, we overlaid circulation patterns at 500 and 850 hPa with trajectories at different altitudes, representing mid-to-upper and low-level flows, respectively. Specifically, trajectories with average altitudes above 3000 m were analyzed at 500 hPa, and those below 3000 m at 850 hPa. This analysis revealed three phases of moisture transport, each controlled by different synoptic systems. From 19 to 23 October, mid-to-upper-level systems—including the midlatitude westerlies and a low-pressure system over the Mediterranean—transported air parcels eastward toward the Mediterranean (Fig. 3(a)). At lower levels, a high-pressure system over the eastern Mediterranean guided moist air toward the southern Mediterranean coast (Fig. 3(b)). From 24 to 25 October, the Mediterranean low weak-

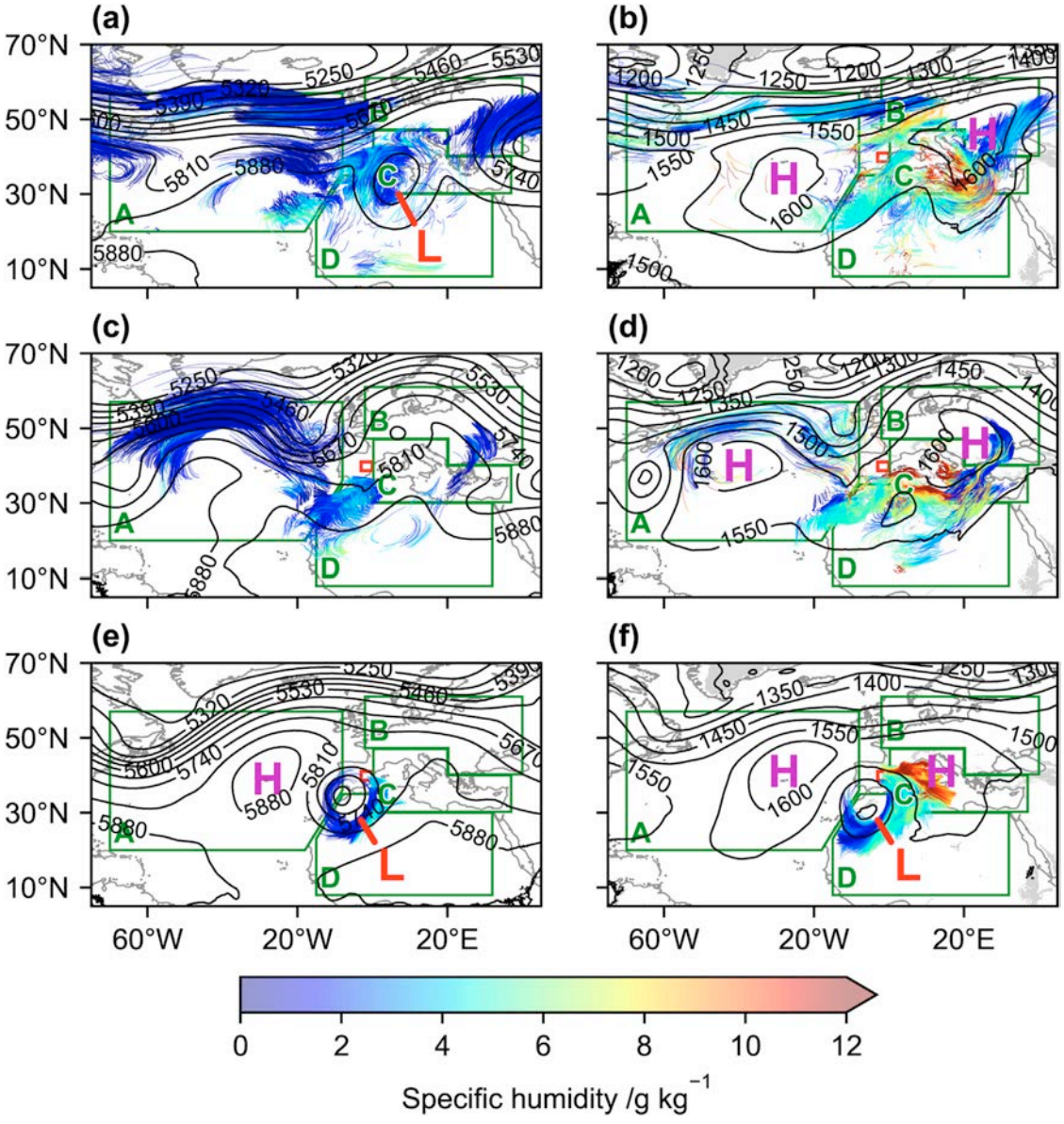

Fig. 3. Geopotential height with air parcel trajectories at different altitudes on 21, 24, and 28 October 2024. Panels (a, c, e) show circulations at 500 hPa, and (b, d, f) at 850 hPa. Panels (a, b) correspond to 21 October 2024; (c, d) to 24 October; and (e, f) to 28 October. Black contours represent geopotential height, and colored trajectories indicate specific humidity. Trajectories are grouped by average height: above 3000 m in (a, c, e), and below 3000 m in (b, d, f). Moisture source regions (A–D) are outlined in green, and the target rainfall region (T) is highlighted in red. The gray shading in (b, d, f) indicates terrain elevation >1500 m. "H" and "L" denote the centers of high-pressure and low-pressure systems, respectively.

ened, and a westerly trough-ridge pattern began to dominate the mid-to-upper levels (Fig. 3(c)). Meanwhile, at low levels, high-pressure systems over the eastern Atlantic and Mediterranean channeled moisture toward the Iberian Peninsula (Fig. 3(d)). Between 26 and 29 October, a deep cut-off low developed and dominated the entire troposphere over Spain. Working in tandem with a subtropical high to the east of Spain, this configuration efficiently funneled moisture from the western Mediterranean toward Valencia (Fig. 3(e, f)).

In summary, moisture transport primarily occurred in the mid- to lower troposphere, with systems to the west (a Mediterranean low and the Atlantic subtropical high) and east (a cut-off low and the eastern Mediterranean high) controlling moisture flow from both directions. Their convergence over Valencia triggered the extreme rainfall. Despite structural differences, these systems worked together to facilitate the moisture transport from the Mediterranean, which played a crucial role in the event.

6. Discussion and conclusion

From 26 October to 2 November 2024, Spain experienced a prolonged period of intense rainfall, which affected nearly the entire country. On 29 October, Turis station in Valencia recorded a record-breaking 710.8 mm of rain within 24 h—exceeding the region's typical annual rainfall. This extreme event caused severe flooding, widespread infrastructure damage, and economic losses exceeding $11 billion. Tragically, 232 lives were lost and many residents were displaced. Synoptic analysis reveals that the primary weather system responsible for this event was a deep, vertically extending cut-off low centered over Spain, flanked by powerful high-pressure systems to the west and east. This configuration caused the low to remain quasi-stationary over the region, enhancing upper-level divergence, mid-level warm advection, and the development of a strong southeasterly low-level jet. These processes promoted sustained upward motion and a continuous supply of moisture. Addi-

tionally, the funnel-shaped topography along the eastern Iberian coast played a critical role in triggering and amplifying convection through forced orographic lifting. Such atmospheric configurations are commonly associated with extreme rainfall events in Spain and the broader Mediterranean region (Ferreira, 2021; Insua-Costa et al., 2021). However, the intensity and societal impact of this event were particularly exceptional, raising concerns about the increasing likelihood of similar or more severe events under a warming climate.

The occurrence of this extreme rainfall event was closely linked to regional and nearby moisture sources. Using Lagrangian trajectory analysis, we traced the moisture transport pathways and quantified the contribution from different source regions. Results show that the Mediterranean was the dominant contributor, accounting for 78.1 % of the moisture, due to its high moisture uptake and minimal transport losses. The regions of northwestern Africa and central-eastern Europe/the Black Sea also contributed significantly, at 8.5 % and 6.2 %, respectively. In contrast, the distant Atlantic only contributed 1.4 % of the moisture, indicating that long-distance transport played a negligible direct role. These results differ from those gained using Eulerian methods, such as those of Insua-Costa et al. (2019), who emphasized the role of moisture advection from the tropical and subtropical Atlantic and Africa in similar extreme events. Furthermore, our estimate of the Mediterranean contribution far exceeds the 20 % reported by Turato et al. (2004) for the 2000 Piedmont floods. This discrepancy may be partly attributable to enhanced evaporation from an anomalously warm Mediterranean in October 2024 (Fig. S3 in the Supplementary Material), possibly linked to ongoing global warming (Pastor et al., 2018; Sánchez-Almodóvar et al., 2022), and warrants further exploration.

In terms of the weather systems controlling moisture transport, the cut-off low and the subtropical high over eastern Spain played key roles in channeling moisture from the Mediterranean and North Africa toward Spain at low levels. Meanwhile, a low-pressure system over the Mediterranean and the subtropical Atlantic high guided mid-to-upper-level trajectories into Spain, which subsequently descended and transformed into warm and moist low-level flows (Fig. S4 in the Supplementary Material). These systems acted in sequence to relay moisture toward the Valencia region, ultimately fueling the extreme rainfall event. A similar relay-like moisture transport process was also observed in an extreme rainfall event in China (Huang et al., 2025).

In summary, this study explains the causes of the extreme rainfall event from the perspectives of synoptic-scale circulation, moisture transport characteristics, and the weather systems controlling that transport. The findings help clarify the key features of this sudden and devastating event in Spain, deepen our understanding of extreme rainfall mechanisms in the Mediterranean and surrounding regions, and provide useful insight for improving heavy rainfall forecasting and early warning systems in other coastal cities with similar funnel-shaped terrain.

Funding

This research was supported by the National Natural Science Foundation of China (42475008) and Strategy Priority Research Program of Chinese Academy of Sciences (XDB0760400).

Acknowledgments

The authors would like to thank the Spanish Meteorological Agency and the European Centre for Medium-Range Weather Forecasts for providing the data.

Supplementary materials

Supplementary material associated with this article can be found, in the online version, at doi:10.1016/j.aosl.2025.100666.

References

Amengual, A., 2022. Hydrometeorological analysis of the 12 and 13 September 2019 widespread flash flooding in eastern Spain. Nat. Hazards Earth Syst. Sci. 22 (4), 1159–1179. doi:10.5194/nhess-22-1159-2022.

Barredo, J.I., 2007. Major flood disasters in Europe: 1950–2005. Nat. Hazard. 42 (1), 125–148. doi:10.1007/s11069-006-9065-2.

Beneto, P., Khodayar, S., 2023. On the need for improved knowledge on the regional-to-local precipitation variability in eastern Spain under climate change. Atmos. Res. 290, 106795. doi:10.1016/j.atmosres.2023.106795.

Drumond, A., Nieto, R., Gimeno, L., Vicente-Serrano, S.M., Lopez-Moreno, J.I., Moran-Tejeda, E., 2011. Characterization of the atmospheric component of the winter hydrological cycle in the Galicia/North Portugal Euro-region: A Lagrangian approach. Clim. Res. 48 (2–3), 193–201. doi:10.3354/cr00987.

Ferreira, R.N., 2021. Cut-off lows and extreme precipitation in eastern Spain: Current and future climate. Atmosphere 12 (7), 835. doi:10.3390/atmos12070835.

Fu, S.M., Sun, J.H., Luo, Y.L., Zhang, Y.C., 2017. Formation of long-lived summertime mesoscale vortices over central East China: Semi-idealized simulations based on a 14-year vortex statistic. J. Atmos. Sci. 74 (12), 3955–3979. doi:10.1175/jas-D-16-0328.1.

Gimeno, L., Nieto, R., Trigo, R.M., Vicente-Serrano, S.M., López-Moreno, J.I., 2010. Where does the Iberian Peninsula moisture come from? An answer based on a Lagrangian approach. J. Hydrometeorol. 11 (2), 421–436. doi:10.1175/2009JHM1182.1.

Hermoso, A., Homar, V., Amengual, A., 2021. The sequence of heavy precipitation and flash flooding of 12 and 13 September 2019 in eastern Spain. Part I: Mesoscale diagnostic and sensitivity analysis of precipitation. J. Hydrometeorol. 22 (5), 1117–1138. doi:10.1175/jhm-D-20-0182.1.

Hersbach, H., Bell, B., Berrisford, P., Hirahara, S., Horanyi, A., Munoz-Sabater, J., Nicolas, J., et al., 2020. The ERA5 global reanalysis. Q. J. R. Meteorol. Soc. 146 (730), 1999–2049. doi:10.1002/qj.3803.

Holton, J.R., Hakim, G.J., 2013a. Chapter 2 - basic conservation laws. In: Holton, J.R., Hakim, G.J. (Eds.), An Introduction to Dynamic Meteorology (fifth edition). Academic Press, Boston, pp. 31–66. doi:10.1016/B978-0-12-384866-6.00002-7.

Holton, J.R., Hakim, G.J., 2013b. Chapter 6 - quasi-geostrophic analysis. In: Holton, J.R., Hakim, G.J. (Eds.), An Introduction to Dynamic Meteorology (fifth edition). Academic Press, Boston, pp. 171–211. doi:10.1016/B978-0-12-384866-6.00006-4.

Huang, T.T., Fu, S.M., Jin, S.L., Liu, X.L., Sun, J.H., Xiao, X., 2025. Unique moisture transport under abnormal circulations for producing the extreme rainstorm over Beijing on July 31, 2023. Q. J. R. Meteorol. Soc. e4955. doi:10.1002/qj.4955.

Huang, T.T., Fu, S.M., Wang, Z.G., Zhao, S., Sun, J.H., Zhang, Y., Wang, S.H., 2024. A case study on the rainstorm-producing mesoscale vortices in central-eastern China. J. Geophys. Res. 129 (5), e2023JD039573. doi:10.1029/2023jd039573.

Insua-Costa, D., Miguez-Macho, G., Carmen Llasat, M., 2019. Local and remote moisture sources for extreme precipitation: A study of the two catastrophic 1982 western Mediterranean episodes. Hydrol. Earth Syst. Sci. 23 (9), 3885–3900. doi:10.5194/hess-23-3885-2019.

Insua-Costa, D., Lemus-Canovas, M., Miguez-Macho, G., Carmen Llasat, M., 2021. Climatology and ranking of hazardous precipitation events in the western Mediterranean area. Atmos. Res. 255, 105521. doi:10.1016/j.atmosres.2021.105521.

Javier Miro, J., Lemus-Canovas, M., Serrano-Notivoli, R., Olcina Cantos, J., Estrela, M.J., Martin-Vide, J., Sarricolea, P., Meseguer-Ruiz, O., 2022. A component-based approximation for trend detection of intense rainfall in the Spanish Mediterranean coast. Wea. Clim. Extrem. 38, 100513. doi:10.1016/j.wace.2022.100513.

Khodayar, S., Kalthoff, N., Kottmeier, C., 2018. Atmospheric conditions associated with heavy precipitation events in comparison to seasonal means in the western Mediterranean region. Clim. Dyn. 51 (3), 951–967. doi:10.1007/s00382-016-3058-y.

Pastor, F., Antonio Valiente, J., Luis Palau, J., 2018. Sea surface temperature in the Mediterranean: trends and spatial patterns (1982–2016). Pure Appl. Geophys. 175 (11), 4017–4029. doi:10.1007/s00024-017-1739-z.

Portugues-Molla, I., Bonache-Felici, X., Mateu-Belles, J.F., Marco-Segura, J.B., 2016. A GIS-based model for the analysis of an urban flash flood and its hydrogeomorphic response. The Valencia event of 1957. J. Hydrol. 541, 582–596. doi:10.1016/j.jhydrol.2016.05.048.

Puertes, C., Francés García, F., 2016. The 1957 Valencia flood: Hydrological and sedimentological reconstruction and comparison to the current situation. Ing. Agua. 20 (4), 181–199. doi:10.4995/ia.2016.4772.

Quante, M., Matthias, V., 2006. Water in the earth's atmosphere. J. Phys. IV 139, 37–61. doi:10.1051/jp4:2006139005.

Ricard, D., Ducrocq, V., Auger, L., 2012. A climatology of the mesoscale environment associated with heavily precipitating events over a northwestern Mediterranean area. J. Appl. Meteorol. Climatol. 51 (3), 468–488. doi:10.1175/jamc-D-11-017.1.

Riesco Martin, J., Mora Garcia, M., de Pablo Davila, F., Rivas Soriano, L., 2013. Severe rainfall events over the western Mediterranean Sea: A case study. Atmos. Res. 127, 47–63. doi:10.1016/j.atmosres.2013.03.001.

Sánchez-Almodóvar, E., Martin-Vide, J., Olcina-Cantos, J., Lemus-Canovas, M., 2022. Are atmospheric situations now more favourable for heavy rainfall in the Spanish Mediterranean? Analysis of episodes in the Alicante province (1981–2020). Atmosphere 13 (9), 1410. doi:10.3390/atmos13091410.

Stohl, A., James, P., 2004. A lagrangian analysis of the atmospheric branch of the global water cycle. Part I: Method description, validation, and demonstration for the August 2002 flooding in central Europe. J. Hydrometeorol. 5 (4), 656–678. doi:10.1175/1525-7541(2004)005<0656:ALAOTA>2.0.CO;2.

Stohl, A., James, P., 2005. A lagrangian analysis of the atmospheric branch of the global water cycle. Part II: Moisture transports between earth's ocean basins and river catchments. J. Hydrometeorol. 6 (6), 961–984. doi:10.1175/jhm470.1.

Stohl, A., Forster, C., Sodemann, H., 2008. Remote sources of water vapor forming precipitation on the Norwegian west coast at 60°N–a tale of hurricanes and an atmospheric river. J. Geophys. Res. 113 (D5), 102. doi:10.1029/2007jd009006.

Sun, B., Wang, H.J., 2014. Moisture sources of semiarid grassland in China using the lagrangian particle model FLEXPART. J. Clim. 27 (6), 2457–2474. doi:10.1175/jcli-d-13-00517.1.

Tao, S.Y., 1980. Rainstorms in China. Science Press, Beijing, 17pp.

Trenberth, K.E., Stepaniak, D.P., 2003. Covariability of components of poleward atmospheric energy transports on seasonal and interannual timescales. J. Clim. 16 (22), 3691–3705. doi:10.1175/1520-0442(2003)016<3691:Cocopa>2.0.Co;2.

Turato, B., Reale, O., Siccardi, F., 2004. Water vapor sources of the October 2000 piedmont flood. J. Hydrometeorol. 5 (4), 693–712. doi:10.1175/1525-7541(2004)005<0693:Wvsoto>2.0.Co;2.